AIAA JOURNAL
Vol. 45, No. 8, August 2007

Constrained-Layer Damping with Gradient Polymers for Effectiveness over Broad Temperature Ranges

Farhan Gandhi*
Pennsylvania State University, University Park, Pennsylvania 16802
Chrystel Remillat† and Geof Tomlinson‡
University of Sheffield, Sheffield S1 3JD England, United Kingdom
and
Julien Austruy§
Institut Supérieur de Mécanique de Paris, 93407 Saint Ouen Cedex, France

DOI: 10.2514/1.19574

The effectiveness of a constrained-layer damping treatment in dissipating energy and thereby augmenting the system damping is contingent on the viscoelastic polymer having a fairly significant value of material loss factor. A monolithic viscoelastic polymer tends to be lossy over a fairly narrow temperature range, corresponding to the material being in the transition state. At temperatures below this range, the viscoelastic polymer displays glassy behavior, whereas for higher temperatures, it displays rubbery behavior. In either case, the material loss factor reduces sharply and the effectiveness of the damping treatment is severely degraded. A gradient viscoelastic polymer layer, for which the properties vary through the thickness of the layer, can increase the temperature range of effectiveness of the damping treatment. This is because different regions through the thickness enter transition at different temperatures, and so the gradient polymer as a whole provides damping augmentation over a broader temperature range. Classical constrained-layer damping treatments with monolithic polymeric damping layers routinely assume a uniform shear strain through the thickness of the damping layer. However, because the shear modulus of the gradient viscoelastic polymer can vary by up to two–three orders of magnitude through the thickness, the shear strain can also be expected to vary substantially through the thickness. Consequently, a new analysis is developed with the gradient viscoelastic polymer modeled as comprising N discrete sublayers, each with its distinct properties and each assigned an independent shear degree of freedom. Simulation results are presented for a gradient polymer comprising $N = 2$ discrete sublayers. The results of the study are used to understand the underlying physics. It is seen that ideally, the glassy temperature of the two sublayers should be approximately similar. Further, the treatment is most effective if the sublayer that goes into glass transition at higher temperatures has a lower rubbery modulus than the sublayer going into glass transition at lower temperatures.

I. Introduction

FREE-LAYER and constrained-layer damping treatments have been widely used for structural-damping-augmentation applications. The latter are particularly effective and nominally comprise a viscoelastic-damping-polymer layer on the surface of the host structure, which is in turn covered by a stiff constraining layer. As the host structure undergoes cyclic deformation, the viscoelastic polymer then undergoes cyclic shear strain and dissipates energy. If the constraining layer is itself an active piezoelectric layer, the energy dissipation (and structural damping) can be further increased. There has been much work in this area in recent years (see, for example, [1–9]). The effectiveness of a constrained-layer damping treatment in dissipating energy and thereby augmenting the system damping is contingent on the viscoelastic polymer having a fairly significant value of material loss factor, or being lossy (in addition to dependence on a number of other design parameters). Unfortunately, when a monolithic viscoelastic polymer is used, as is the case in classical damping treatments, the material is lossy over a fairly narrow temperature range (typically around 40–60°F), corresponding to the polymer transitioning from the glassy to the rubbery state. At temperatures below this range, the viscoelastic polymer displays glassy behavior, whereas for higher temperatures, it displays rubbery behavior. In both cases, the material loss factor reduces sharply and its effectiveness as a damping treatment is severely degraded. Using polymer blends and multilayer treatments are a couple of possible methods for improving the temperature range of effectiveness [10–13]. Recently, the second and third authors of this article suggested the use of a gradient viscoelastic polymer, for which the properties vary through the thickness of the layer [14,15]. Like multilayer treatments, the improved effectiveness of a gradient viscoelastic polymer over a broad temperature range is based on different regions through the thickness providing high damping over different temperature ranges.

Use of gradient viscoelastic polymers or multiple polymer layers in damping treatments presents an interesting set of modeling challenges. In the analysis of classical constrained-layer damping treatments with a monolithic polymeric damping material, it is routinely assumed that the shear strain through the thickness of the damping layer is uniform. However, with a gradient viscoelastic polymer, the shear modulus can vary by as much as two–three orders of magnitude through the thickness. Because of the large variation in shear modulus through the thickness, the shear strain can also be expected to vary substantially, and the uniform-shear-strain assumption used for monolithic treatments would no longer be valid.

This paper describes a new analysis developed in which a gradient viscoelastic polymer of a constrained-layer damping treatment is

Received 22 August 2005; revision received 28 December 2006; accepted for publication 28 December 2006.

*Professor, Aerospace Engineering Department, 229 Hammond Building, Senior Member AIAA.
†Currently Lecturer, Aerospace Engineering Department, University of Bristol, England, United Kingdom.
‡Professor, Mechanical Engineering, Pro-Vice Chancellor (Research), Mappin Building.
§Visiting Researcher, Pennsylvania State University, Aerospace Engineering Department.

modeled as comprising N discrete sublayers, each with its distinct properties and each assigned an independent shear degree of freedom ($\gamma_1, \gamma_2, \gamma_3, \ldots, \gamma_N$), to represent the shear strain variation through the thickness. As the temperature varies, different regions through the thickness will be in the glassy, rubbery, or transition (dissipative) state. The shear modulus will correspondingly vary, accompanied by significant through-the-thickness variations in shear strain, at different temperatures. Because the energy dissipation and damping performance characteristics of the gradient (or multilayer) polymer treatment are strongly dependent on the shear strain levels in the dissipative regions within the polymer, it is critical to accurately model the shear strain distribution through the thickness. The model developed in this paper provides the capability to rigorously analyze the performance of such a gradient-polymer damping treatment. Results from the analysis are then used to develop an understanding of desirable characteristics of the gradient viscoelastic polymer so as to improve its effectiveness as a broad-temperature damping treatment. Demonstration of damping augmentation over a broad temperature range using two properly selected commercially available damping materials as sublayers of the constrained viscoelastic layer is also provided.

II. Analytical Model and Solution Scheme

In this section, the kinematics of deformation, layer-by-layer expressions for strain, and variations in the strain energy and kinetic energy are derived for beams with gradient viscoelastic treatments on the upper and lower surfaces, covered by constraining layers. The beam is discretized using the finite element method, and the element stiffness and mass matrices are derived from the expressions for strain energy and kinetic energy variations. After assembly, the global differential equations of motion can be obtained. Because the viscoelastic material behavior is described using the complex modulus, the system-governing differential equations are solved in the frequency domain. The modal loss factor is calculated as a measure of the modal damping. This entire process is described in detail in the subsections that follow.

A. Finite Element Equations of Motion

1. Kinematics of Deformation

Figure 1 shows a section of the beam in the deformed configuration, where $\partial w/\partial x$ is the slope of the beam, and $\gamma_1, \gamma_2, \gamma_3, \ldots, \gamma_N$ are the shear angles in the N sublayers of the viscoelastic material. From the figure, expressions for the axial displacements in the individual layers can be obtained. The axial displacement in the base beam is

$$u_b = -z\frac{\partial w}{\partial x} \tag{1}$$

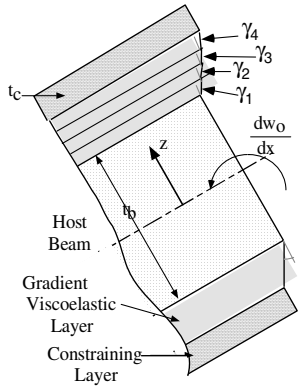

Fig. 1 Constrained-layer damping treatment with gradient viscoelastic polymer modeled using N discrete sublayers.

The axial displacements in the viscoelastic sublayers are

First sublayer (adjacent to the base beam), top:

$$u^{1t} = -z\frac{\partial w}{\partial x} + (z - T_1)\gamma_1 \tag{2a}$$

First sublayer (adjacent to the base beam), bottom:

$$u^{1b} = -z\frac{\partial w}{\partial x} + (z + T_1)\gamma_1 \tag{2b}$$

Second sublayer, top:

$$u^{2t} = -z\frac{\partial w}{\partial x} + t_1\gamma_1 + (z - T_2)\gamma_2 \tag{3a}$$

Second sublayer, bottom:

$$u^{2b} = -z\frac{\partial w}{\partial x} - t_1\gamma_1 + (z + T_2)\gamma_2 \tag{3b}$$

Third sublayer, top:

$$u^{3t} = -z\frac{\partial w}{\partial x} + t_1\gamma_1 + t_2\gamma_2 + (z - T_3)\gamma_3 \tag{4a}$$

Third sublayer, bottom:

$$u^{3b} = -z\frac{\partial w}{\partial x} - t_1\gamma_1 - t_2\gamma_2 + (z + T_3)\gamma_3 \tag{4b}$$

Nth sublayer (adjacent to the constraining layer), top:

$$u^{Nt} = -z\frac{\partial w}{\partial x} + \sum_{k=1}^{N-1} t_k\gamma_k + (z - T_N)\gamma_N \tag{5a}$$

Nth sublayer (adjacent to the constraining layer), bottom:

$$u^{Nb} = -z\frac{\partial w}{\partial x} - \sum_{k=1}^{N-1} t_k\gamma_k + (z + T_N)\gamma_N \tag{5b}$$

In Eqs. (2–5), the parameters $t_1, t_2, t_3, \ldots, t_N$ represent the thickness of each of the N sublayers of the viscoelastic material, and $T_1, T_2, T_3, \ldots, T_N$ represent the distances from the midplane to the bottom of the Nth sublayer of the viscoelastic material. Thus, $T_1 = t_b/2$ (where t_b is the thickness of the base beam), $T_2 = T_1 + t_1$, and $T_3 = T_2 + t_2, \ldots, T_N = T_{N-1} + t_{N-1}$. The axial displacements in the top and bottom constraining layers, respectively, are

Top:

$$u^{ct} = -z\frac{\partial w}{\partial x} + \sum_{k=1}^{N} t_k\gamma_k \tag{6a}$$

Bottom:

$$u^{cb} = -z\frac{\partial w}{\partial x} - \sum_{k=1}^{N} t_k\gamma_k \tag{6b}$$

2. Strains in the Individual Layers

The normal strains in the individual layers can then be obtained by simply differentiating Eqs. (1–6). The normal strain in the base beams is

$$\varepsilon_{xx}^{b} = -z\frac{\partial^2 w}{\partial x^2} \tag{7}$$

The normal strains in the viscoelastic sublayers areFirst sublayer (adjacent to the base beam), top:

$$\varepsilon_{xx}^{1t} = -z\frac{\partial^2 w}{\partial x^2} + (z - T_1)\frac{\partial \gamma_1}{\partial x} \tag{8a}$$

First sublayer (adjacent to the base beam), bottom:

$$\varepsilon_{xx}^{1b} = -z\frac{\partial^2 w}{\partial x^2} + (z + T_1)\frac{\partial \gamma_1}{\partial x} \tag{8b}$$

Second sublayer, top:

$$\varepsilon_{xx}^{2t} = -z\frac{\partial^2 w}{\partial x^2} + t_1\frac{\partial \gamma_1}{\partial x} + (z - T_2)\frac{\partial \gamma_2}{\partial x} \tag{9a}$$

Second sublayer, bottom:

$$\varepsilon_{xx}^{2b} = -z\frac{\partial^2 w}{\partial x^2} - t_1\frac{\partial \gamma_1}{\partial x} + (z + T_2)\frac{\partial \gamma_2}{\partial x} \tag{9b}$$

Third sublayer, top:

$$\varepsilon_{xx}^{3t} = -z\frac{\partial^2 w}{\partial x^2} + t_1\frac{\partial \gamma_1}{\partial x} + t_2\frac{\partial \gamma_2}{\partial x} + (z - T_3)\frac{\partial \gamma_3}{\partial x} \tag{10a}$$

Third sublayer, bottom:

$$\varepsilon_{xx}^{3b} = -z\frac{\partial^2 w}{\partial x^2} - t_1\frac{\partial \gamma_1}{\partial x} - t_2\frac{\partial \gamma_2}{\partial x} + (z + T_3)\frac{\partial \gamma_3}{\partial x} \tag{10b}$$

*N*th sublayer (adjacent to the constraining layer), top:

$$\varepsilon_{xx}^{Nt} = -z\frac{\partial^2 w}{\partial x^2} + \sum_{k=1}^{N-1} t_k\frac{\partial \gamma_k}{\partial x} + (z - T_N)\frac{\partial \gamma_N}{\partial x} \tag{11a}$$

*N*th sublayer (adjacent to the constraining layer), bottom:

$$\varepsilon_{xx}^{Nb} = -z\frac{\partial^2 w}{\partial x^2} - \sum_{k=1}^{N-1} t_k\frac{\partial \gamma_k}{\partial x} + (z + T_N)\frac{\partial \gamma_N}{\partial x} \tag{11b}$$

The normal strains in the top and bottom constraining layers are

Top:

$$\varepsilon_{xx}^{ct} = -z\frac{\partial^2 w}{\partial x^2} + \sum_{k=1}^{N} t_k\frac{\partial \gamma_k}{\partial x} \tag{12a}$$

Bottom:

$$\varepsilon_{xx}^{cb} = -z\frac{\partial^2 w}{\partial x^2} - \sum_{k=1}^{N} t_k\frac{\partial \gamma_k}{\partial x} \tag{12b}$$

The transverse shear strain ε_{zx} is zero for the base beam and the constraining layers. Transverse shear strains in the individual viscoelastic sublayers are $\gamma_1, \gamma_2, \gamma_3, \ldots, \gamma_N$.

3. *Strain Energy Variation*

The strain energy variation δU, with contributions due to flexural and shear deformations, can be written as

$$\begin{aligned}\delta U &= \int_{\text{volume}} (\delta\varepsilon_{xx}\sigma_{xx} + \delta\varepsilon_{xz}\sigma_{xz})\,\mathrm{d}V \\ &= \int_0^L \left\{ \int_{\text{cross section}} \delta\varepsilon_{xx}E(z)\varepsilon_{xx}b\,\mathrm{d}z \right. \\ &\quad \left. + \int_{\text{cross section}} \delta\varepsilon_{zx}G_s(z)\varepsilon_{zx}b\,\mathrm{d}z \right\}\mathrm{d}x\end{aligned} \tag{13}$$

In Eq. (13), Young's modulus E varies from layer to layer (E_b for the base beam, $E_1, E_2, E_3, \ldots, E_N$ for the N sublayers of the viscoelastic material, and E_c for the constraining layer). The viscoelastic sublayers alone contribute to the strain energy variation due to shear deformation (with $G_1, G_2, G_3, \ldots, G_N$ representing the shear moduli of the individual sublayers), whereas the base beam and constraining layer are assumed to be shear-inflexible. Note that $E_1, \ldots, E_N$ and $G_1, \ldots, G_N$ are complex quantities and can vary with both frequency and temperature. Introducing the expressions for strains in the various layers (from Sec. II.A.2) into Eq. (13) and evaluating the integrals over the cross section yields

$$\begin{aligned}\delta U = &\int_0^L \begin{bmatrix} \frac{\partial^2 \delta w}{\partial x^2} & \frac{\partial \delta\gamma_1}{\partial x} & \frac{\partial \delta\gamma_2}{\partial x} & \cdots & \frac{\partial \delta\gamma_N}{\partial x} \end{bmatrix} \\ &\times \begin{bmatrix} C_{ww} & C_{w1} & C_{w2} & \cdots & C_{wN} \\ & C_{11} & C_{12} & \cdots & C_{1N} \\ & & C_{22} & \cdots & C_{2N} \\ & & & \ddots & \vdots \\ & & & & C_{NN} \end{bmatrix} \begin{Bmatrix} \partial^2 w/\partial x^2 \\ \partial\gamma_1/\partial x \\ \partial\gamma_2/\partial x \\ \vdots \\ \partial\gamma_N/\partial x \end{Bmatrix} \mathrm{d}x \\ &+ \int_0^L \begin{bmatrix} \partial\gamma_1 & \partial\gamma_2 & \cdots & \partial\gamma_N \end{bmatrix} 2b \begin{bmatrix} G_1 t_1 & 0 & \cdots & 0 \\ & G_2 t_2 & & 0 \\ & & \ddots & \vdots \\ & & & G_N t_N \end{bmatrix} \\ &\times \begin{Bmatrix} \gamma_1 \\ \gamma_2 \\ \vdots \\ \gamma_N \end{Bmatrix} \mathrm{d}x\end{aligned} \tag{14}$$

where

$$\begin{aligned} C_{ww} &= \frac{E_b b t_b^3}{12} + \frac{2}{3}b\sum_{k=1}^{N} E_k\left[T_{ku}^3 - T_k^3\right] + \frac{2E_c b}{3}\left[\left(\frac{t_b}{2} + t_v + t_c\right)^3 - \left(\frac{t_b}{2} + t_v\right)^3\right] \\ C_{wj} &= E_j b\left[-\frac{2}{3}\left\{T_{ju}^3 - T_j^3\right\} + T_j\left\{T_{ju}^2 - T_j^2\right\}\right] - \sum_{k=j+1}^{N} E_k b t_j[T_{ku}^2 - T_k^2] - E_c b t_j\left[\left(\frac{t_b}{2} + t_v + t_c\right)^2 - \left(\frac{t_b}{2} + t_v\right)^2\right] \quad \text{for } j = 1, \ldots, N \\ C_{ii} &= E_i b\left(\frac{2t_i^3}{3}\right) + 2bt_i^2\sum_{k=i+1}^{N} E_k t_k + 2E_c b t_i^2 t_c \quad \text{for } i = 1, \ldots, N \\ C_{ij} &= E_j b t_i\left[\left\{T_{ju}^2 - T_j^2\right\} - 2T_j t_j\right] + 2bt_i t_j\sum_{k=j+1}^{N} E_k t_k + 2E_c b t_i t_j t_c \\ &\quad \text{for } i = 1, \ldots, N, \quad \text{and} \quad j = i+1, \ldots, N \end{aligned} \tag{15}$$

In Eq. (15),

$$t_v = \sum_{k=1}^{N} t_k$$

represents the total thickness of the viscoelastic material on the upper or lower surfaces of the beam (as the sum of each of the thickness of each of the N sublayers), t_c is the thickness of the constraining layer, and T_{ku} represents the offset from the neutral axis to the top surface of the kth viscoelastic sublayer ($T_{ku} = T_k + t_k$).

4. *Kinetic Energy Variation*

The variation in kinetic energy δT can be written as

$$\delta T = \int_0^L m\delta\dot{w}\,\dot{w}\;\mathrm{d}x + \int_0^L \left\{ \int_{\text{cross section}} \varsigma(z)b\delta\dot{u}\,\dot{u}\,dz \right\}\mathrm{d}x \tag{16}$$

The first and second terms, respectively, represent kinetic energy variations due to transverse w motion and longitudinal u motion. Differentiating the expressions in Sec. II.A.1 with respect to time to obtain the axial velocities in the individual layers and evaluating the

integral over the cross section yields

$$\delta T = \int_0^L \delta\dot{w} m \dot{w}\, \mathrm{d}x + \int_0^L \lfloor \tfrac{\partial\delta\dot{w}}{\partial x} \quad \delta\dot{\gamma}_1 \quad \delta\dot{\gamma}_2 \quad \cdots \quad \delta\dot{\gamma}_N \rfloor \begin{bmatrix} \tau_{ww} & \tau_{w1} & \tau_{w2} & \cdots & \tau_{wN} \\ & \tau_{11} & \tau_{12} & \cdots & \tau_{1N} \\ & & \tau_{22} & \cdots & \tau_{2N} \\ & & & \ddots & \vdots \\ & & & & \tau_{NN} \end{bmatrix} \begin{Bmatrix} \frac{\partial\dot{w}}{\partial x} \\ \dot{\gamma}_1 \\ \dot{\gamma}_2 \\ \vdots \\ \dot{\gamma}_N \end{Bmatrix} \mathrm{d}x \tag{17}$$

where

$$\begin{aligned}
\tau_{ww} &= \frac{\rho_b b t_b^3}{12} + \frac{2}{3} b \sum_{k=1}^{N} \rho_k [T_{ku}^3 - T_k^3] + \frac{2\rho_c b}{3}\left[\left(\frac{t_b}{2} + t_v + t_c\right)^3 - \left(\frac{t_b}{2} + t_v\right)^3\right] \\
\tau_{wj} &= \rho_j b\left[-\frac{2}{3}\{T_{ju}^3 - T_j^3\} + T_j\{T_{ju}^2 - T_j^2\}\right] - \sum_{k=j+1}^{N} \rho_k b t_j [T_{ku}^2 - T_k^2] - \rho_c b t_j\left[\left(\frac{t_b}{2} + t_v + t_c\right)^2 - \left(\frac{t_b}{2} + t_v\right)^2\right] \quad \text{for } j = 1, \ldots, N \\
\tau_{ii} &= \rho_i b\left(\frac{2t_i^3}{3}\right) + 2bt_i^2 \sum_{k=i+1}^{N} \rho_k t_k + 2\rho_c b t_i^2 t_c \quad \text{for } i = 1, \ldots, N \\
\tau_{ij} &= \rho_j b t_i [\{T_{ju}^2 - T_j^2\} - 2T_j t_j] + 2bt_i t_j \sum_{k=j+1}^{N} \rho_k t_k + 2\rho_c b t_i t_j t_c \quad \text{for } i = 1, \ldots, N, \quad \text{and} \quad j = i+1, \ldots, N
\end{aligned} \tag{18}$$

with $\rho_b, \rho_1, \rho_2, \rho_3, \ldots, \rho_N$, and ρ_c denoting the mass densities of the base beam, the N viscoelastic sublayers, and constraining layer, respectively.

5. *Finite Element Discretization*

The equations of motion are obtained by using expressions for strain energy variation [Eq. (14)] and kinetic energy variation [Eq. (17)] in the Hamilton's principle and discretizing the structure using the finite element method (Fig. 2). Over the length of any individual element, the transverse displacement w and the shear in the individual sublayers $\gamma_1, \gamma_2, \gamma_3, \ldots, \gamma_N$ are assumed to vary as follows:

$$w = N_{w_l} w_l + N_{\theta_l} \theta_l + N_{w_r} w_r + N_{\theta_r} \theta_r \tag{19}$$

and

$$\begin{aligned}
\gamma_1 &= N_l \gamma_{1l} + N_r \gamma_{1r} \\
\gamma_2 &= N_l \gamma_{2l} + N_r \gamma_{2r} \\
\gamma_3 &= N_l \gamma_{3l} + N_r \gamma_{3r} \\
&\vdots \\
\gamma_N &= N_l \gamma_{Nl} + N_r \gamma_{Nr}
\end{aligned} \tag{20}$$

where w_l and θ_l are the transverse displacement and rotation at the left-end node of the element, w_r and θ_r are corresponding values at the right end; $\gamma_{1l}, \gamma_{2l}, \gamma_{3l}, \ldots, \gamma_{Nl}$ are the shear angles in the various viscoelastic sublayers at the left end of the element, and $\gamma_{1r}, \gamma_{2r}, \gamma_{3r}, \ldots, \gamma_{Nr}$ are the corresponding shear angles at the right end of the element (see Fig. 2). The shape functions in Eqs. (19) and (20) are

$$\lfloor N_{w_l} \quad N_{\theta_l} \quad N_{w_r} \quad N_{\theta_r} \rfloor = \lfloor\, 1 - 3\xi^2 + 2\xi^3 \quad (-\xi + 2\xi^2 - \xi^3)l \quad 3\xi^2 - 2\xi^3 \quad (\xi^2 - \xi^3)l \,\rfloor \quad \text{and} \quad \lfloor N_l \quad N_r \rfloor = \lfloor\, (1-\xi) \quad \xi \,\rfloor \tag{21}$$

where ξ is the nondimensional local coordinate within the element ($0 < \xi < 1$), and l is the element length. Further, the $2 \times (2 + N)$ element nodal degree-of-freedom vector $\{q\}$ is defined as

$$\{q\} = \lfloor\, w_1 \quad \theta_1 \quad \gamma_{1l} \quad \gamma_{2l} \quad \gamma_{3l} \quad \cdots \quad \gamma_{Nl} \quad w_2 \quad \theta_2 \quad \gamma_{1r} \quad \gamma_{2r} \quad \gamma_{3r} \quad \cdots \quad \gamma_{Nr} \,\rfloor^T \tag{22}$$

6. *Element Stiffness Matrix*

In Eq. (14) for the strain energy variation, the displacements and their spatial derivatives at any axial location can now be written in terms of the shape functions and nodal displacements. Thus,

$$\begin{Bmatrix} \partial^2 w/\partial x^2 \\ \partial\gamma_1/\partial x \\ \partial\gamma_2/\partial x \\ \vdots \\ \partial\gamma_N/\partial x \end{Bmatrix} = [B_1]\{q\} \quad \text{with} \quad [B_1] = \begin{bmatrix} \frac{1}{l^2}N''_{w_l} & \frac{1}{l^2}N''_{\theta_l} & 0 & 0 & \cdots & 0 & \frac{1}{l^2}N''_{w_r} & \frac{1}{l^2}N''_{\theta_r} & 0 & 0 & \cdots & 0 \\ 0 & 0 & \frac{1}{l}N'_l & 0 & \cdots & 0 & 0 & 0 & \frac{1}{l}N'_r & 0 & \cdots & 0 \\ 0 & 0 & & \frac{1}{l}N'_l & \cdots & 0 & 0 & 0 & & \frac{1}{l}N'_r & \cdots & 0 \\ \vdots & \vdots & & & \ddots & \vdots & \vdots & \vdots & & & \ddots & \vdots \\ 0 & 0 & & & & \frac{1}{l}N'_l & 0 & 0 & & & & \frac{1}{l}N'_r \end{bmatrix} \quad \text{and}$$

$$\begin{Bmatrix} \gamma_1 \\ \gamma_2 \\ \vdots \\ \gamma_N \end{Bmatrix} = [B_2]\{q\} \quad \text{with} \quad [B_2] = \begin{bmatrix} 0 & 0 & N_l & 0 & \cdots & 0 & 0 & 0 & N_r & 0 & \cdots & 0 \\ 0 & 0 & & N_l & \cdots & 0 & 0 & 0 & & N_r & \cdots & 0 \\ \vdots & \vdots & & & \ddots & \vdots & \vdots & \vdots & & & \ddots & \vdots \\ 0 & 0 & & & & N_l & 0 & 0 & & & & N_r \end{bmatrix} \tag{23}$$

Introducing Eqs. (23) into Eq. (14) and integrating along the element length yields the $(4 + 2N) \times (4 + 2N)$ element stiffness matrix K:

$$K = \int_0^1 [B_1]^T \begin{bmatrix} C_{ww} & C_{w1} & C_{w2} & \cdots & C_{wN} \\ & C_{11} & C_{12} & \cdots & C_{1N} \\ & & C_{22} & \cdots & C_{2N} \\ & & & \ddots & \vdots \\ & & & & C_{NN} \end{bmatrix} [B_1] l \, \mathrm{d}\xi + \int_0^1 [B_2]^T 2b \begin{bmatrix} G_1 t_1 & 0 & \cdots & 0 \\ & G_2 t_2 & & 0 \\ & & \ddots & \vdots \\ & & & G_N t_N \end{bmatrix} [B_2] l \, \mathrm{d}\xi$$

$$K = \begin{bmatrix} \frac{12}{l^3} C_{ww} & -\frac{6}{l^2} C_{ww} & 0 & 0 & \cdots & 0 & -\frac{12}{l^3} C_{ww} & -\frac{6}{l^2} C_{ww} & 0 & 0 & \cdots & 0 \\ & \frac{4}{l} C_{ww} & -\frac{1}{l} C_{w1} & -\frac{1}{l} C_{w2} & \cdots & -\frac{1}{l} C_{wN} & \frac{6}{l^2} C_{ww} & \frac{2}{l} C_{ww} & \frac{1}{l} C_{w1} & \frac{1}{l} C_{w2} & \cdots & \frac{1}{l} C_{wN} \\ & & \frac{1}{l} C_{11} & \frac{1}{l} C_{12} & \cdots & \frac{1}{l} C_{1N} & 0 & \frac{1}{l} C_{w1} & -\frac{1}{l} C_{11} & -\frac{1}{l} C_{12} & \cdots & -\frac{1}{l} C_{1N} \\ & & & \frac{1}{l} C_{22} & \cdots & \frac{1}{l} C_{2N} & 0 & \frac{1}{l} C_{w2} & -\frac{1}{l} C_{12} & -\frac{1}{l} C_{22} & \cdots & -\frac{1}{l} C_{2N} \\ & & & & \ddots & \vdots & \vdots & \vdots & \vdots & \vdots & \ddots & \vdots \\ & & & & & \frac{1}{l} C_{NN} & 0 & \frac{1}{l} C_{wN} & -\frac{1}{l} C_{1N} & -\frac{1}{l} C_{2N} & \cdots & -\frac{1}{l} C_{NN} \\ & & & & & & \frac{12}{l^3} C_{ww} & \frac{6}{l^2} C_{ww} & 0 & 0 & \cdots & 0 \\ & & & & & & & \frac{4}{l} C_{ww} & -\frac{1}{l} C_{w1} & -\frac{1}{l} C_{w2} & \cdots & -\frac{1}{l} C_{wN} \\ & & & & & & & & \frac{1}{l} C_{11} & \frac{1}{l} C_{12} & \cdots & \frac{1}{l} C_{1N} \\ & & & & & & & & & \frac{1}{l} C_{22} & \cdots & \frac{1}{l} C_{2N} \\ & & & & & & & & & & \ddots & \vdots \\ & & & & & & & & & & & \frac{1}{l} C_{NN} \end{bmatrix}$$

$$+ \begin{bmatrix} 0 & 0 & 0 & 0 & \cdots & 0 & 0 & 0 & 0 & 0 & \cdots & 0 \\ & 0 & 0 & 0 & \cdots & 0 & 0 & 0 & 0 & 0 & \cdots & 0 \\ & & \frac{2}{3} blG_1 t_1 & 0 & \cdots & 0 & 0 & 0 & \frac{1}{3} blG_1 t_1 & 0 & \cdots & 0 \\ & & & \frac{2}{3} blG_2 t_2 & \cdots & 0 & 0 & 0 & 0 & \frac{1}{3} blG_2 t_2 & \cdots & 0 \\ & & & & \ddots & \vdots & \vdots & \vdots & \vdots & \vdots & \ddots & \vdots \\ & & & & & \frac{2}{3} blG_N t_N & 0 & 0 & 0 & 0 & \cdots & \frac{1}{3} blG_N t_N \\ & & & & & & 0 & 0 & 0 & 0 & \cdots & 0 \\ & & & & & & & 0 & 0 & 0 & \cdots & 0 \\ & & & & & & & & \frac{2}{3} blG_1 t_1 & 0 & \cdots & 0 \\ & & & & & & & & & \frac{2}{3} blG_2 t_2 & \cdots & 0 \\ & & & & & & & & & & \ddots & \vdots \\ & & & & & & & & & & & \frac{2}{3} blG_N t_N \end{bmatrix} \tag{24}$$

7. Element Mass Matrix

In Eq. (17) for the kinetic energy variation, the velocities and their spatial derivatives at any axial location can similarly be written in terms of the shape functions and nodal displacements. Thus,

$$\dot{w}_o = [B_3]\{\dot{q}\} \quad \text{with} \quad [B_3] = \begin{bmatrix} N_{w_l} & N_{\theta_l} & 0 & 0 & \cdots & 0 & N_{w_r} & N_{\theta_r} & 0 & 0 & \cdots & 0 \end{bmatrix} \tag{25}$$

and

$$\begin{Bmatrix} \frac{\partial \dot{w}}{\partial x} \\ \dot{\gamma}_1 \\ \dot{\gamma}_2 \\ \vdots \\ \dot{\gamma}_N \end{Bmatrix} = [B_4]\{\dot{q}\}$$

with

$$[B_4] = \begin{bmatrix} \frac{1}{l} N'_{w_l} & \frac{1}{l} N'_{\theta_l} & 0 & 0 & \cdots & 0 & \frac{1}{l} N'_{w_r} & \frac{1}{l} N'_{\theta_r} & 0 & 0 & \cdots & 0 \\ 0 & 0 & N_l & 0 & \cdots & 0 & 0 & 0 & N_r & 0 & \cdots & 0 \\ 0 & 0 & & N_l & \cdots & 0 & 0 & 0 & & N_r & \cdots & 0 \\ \vdots & \vdots & & & \ddots & \vdots & \vdots & \vdots & & & \ddots & \vdots \\ 0 & 0 & & & & N_l & 0 & 0 & & & & N_r \end{bmatrix}$$

Introducing Eqs. (25) into Eq. (17) and integrating along the element length yields the $(4 + 2N) \times (4 + 2N)$ element mass matrix M:

$$M = \int_0^1 [B_3]^T m [B_3] l \, \mathrm{d}\xi + \int_0^1 [B_4]^T \begin{bmatrix} \tau_{ww} & \tau_{w1} & \tau_{w2} & \cdots & \tau_{wN} \\ & \tau_{11} & \tau_{12} & \cdots & \tau_{1N} \\ & & \tau_{22} & \cdots & \tau_{2N} \\ & & & \ddots & \vdots \\ & & & & \tau_{NN} \end{bmatrix} [B_4] l \, \mathrm{d}\xi$$

$$M = \begin{bmatrix} \frac{36}{30l}\tau_{ww} & -\frac{3}{30}\tau_{ww} & -\frac{1}{2}\tau_{w1} & -\frac{1}{2}\tau_{w2} & \cdots & -\frac{1}{2}\tau_{wN} & -\frac{36}{30l}\tau_{ww} & -\frac{3}{30}\tau_{ww} & -\frac{1}{2}\tau_{w1} & -\frac{1}{2}\tau_{w2} & \cdots & -\frac{1}{2}\tau_{wN} \\ & \frac{4l}{30}\tau_{ww} & -\frac{l}{12}\tau_{w1} & -\frac{l}{12}\tau_{w2} & \cdots & -\frac{l}{12}\tau_{wN} & \frac{3}{30}\tau_{ww} & -\frac{l}{30}\tau_{ww} & \frac{l}{12}\tau_{w1} & \frac{l}{12}\tau_{w2} & \cdots & \frac{l}{12}\tau_{wN} \\ & & \frac{l}{3}\tau_{11} & \frac{l}{3}\tau_{12} & \cdots & \frac{l}{3}\tau_{1N} & \frac{1}{2}\tau_{w1} & \frac{l}{12}\tau_{w1} & \frac{l}{6}\tau_{11} & \frac{l}{6}\tau_{12} & \cdots & \frac{l}{6}\tau_{1N} \\ & & & \frac{l}{3}\tau_{22} & \cdots & \frac{l}{3}\tau_{2N} & \frac{1}{2}\tau_{w2} & \frac{l}{12}\tau_{w2} & \frac{l}{6}\tau_{12} & \frac{l}{6}\tau_{22} & \cdots & \frac{l}{6}\tau_{2N} \\ & & & & \ddots & \vdots & \vdots & \vdots & \vdots & \vdots & \ddots & \vdots \\ & & & & & \frac{l}{3}\tau_{NN} & \frac{1}{2}\tau_{wN} & \frac{l}{12}\tau_{wN} & \frac{l}{6}\tau_{1N} & \frac{l}{6}\tau_{2N} & \cdots & \frac{l}{6}\tau_{NN} \\ & & & & & & \frac{36}{30l}\tau_{ww} & \frac{3}{30}\tau_{ww} & \frac{1}{2}\tau_{w1} & \frac{1}{2}\tau_{w2} & \cdots & \frac{1}{2}\tau_{wN} \\ & & & & & & & \frac{4l}{30}\tau_{ww} & -\frac{l}{12}\tau_{w1} & -\frac{l}{12}\tau_{w2} & \cdots & -\frac{l}{12}\tau_{wN} \\ & & & & & & & & \frac{l}{3}\tau_{11} & \frac{l}{3}\tau_{12} & \cdots & \frac{l}{3}\tau_{1N} \\ & & & & & & & & & \frac{l}{3}\tau_{22} & \cdots & \frac{l}{3}\tau_{2N} \\ & & & & & & & & & & \ddots & \vdots \\ & & & & & & & & & & & \frac{l}{3}\tau_{NN} \end{bmatrix}$$

$$+ \begin{bmatrix} \frac{156ml}{420} & -\frac{22ml^2}{420} & 0 & 0 & \cdots & 0 & \frac{54ml}{420} & \frac{13ml^2}{420} & 0 & 0 & \cdots & 0 \\ & \frac{4ml^3}{420} & 0 & 0 & \cdots & 0 & -\frac{13ml^2}{420} & -\frac{3ml^3}{420} & 0 & 0 & \cdots & 0 \\ & & 0 & 0 & \cdots & 0 & 0 & 0 & 0 & 0 & \cdots & 0 \\ & & & 0 & \cdots & 0 & 0 & 0 & 0 & 0 & \cdots & 0 \\ & & & & \ddots & \vdots & \vdots & \vdots & \vdots & \vdots & \ddots & \vdots \\ & & & & & 0 & 0 & 0 & 0 & 0 & \cdots & 0 \\ & & & & & & \frac{156ml}{420} & \frac{22ml^2}{420} & 0 & 0 & \cdots & 0 \\ & & & & & & & \frac{4ml^3}{420} & 0 & 0 & \cdots & 0 \\ & & & & & & & & 0 & 0 & \cdots & 0 \\ & & & & & & & & & 0 & \cdots & 0 \\ & & & & & & & & & & \ddots & 0 \\ & & & & & & & & & & & 0 \end{bmatrix} \tag{26}$$

8. Global Equations of Motion

The element stiffness and mass matrices can be assembled to produce the global stiffness and mass matrices K_G and M_G. After application of geometric boundary conditions, the system equations of motion can then be written as

$$M_G \ddot{q}_G + K_G q_G = F_G \quad \text{or} \quad M_G \ddot{q}_G + (K'_G + jK''_G) q_G = F_G \tag{27}$$

In the preceding equation, F_G is the external load vector, q_G is the global degree-of-freedom vector, and the global stiffness matrix is complex (of the form $K_G = K'_G + jK''_G$) because of the complex modulus of the viscoelastic material [for example, $G_k = G'_k + jG''_k$ in Eq. (14)].

B. Calculation of System Response

In the present study, the beam is assumed to be simply supported at both ends and subjected to a transverse sinusoidal excitation force at the midpoint. Because the complex modulus approach is used for characterization of the viscoelastic behavior of the gradient-polymer sublayers, the system behavior is examined in the frequency domain using harmonic balance, with the applied force and response expressed as

$$F_G = F_o e^{j\Omega t} \quad \text{and} \quad q_G = \left(q'_G + jq''_G\right) e^{j\Omega t} \tag{28}$$

Introducing Eqs. (28) into Eq. (27), it can be shown that

$$\begin{bmatrix} K'_G - \Omega^2 M_G & -K''_G \\ K''_G & K'_G - \Omega^2 M_G \end{bmatrix} \begin{Bmatrix} q'_G \\ q''_G \end{Bmatrix} = \begin{Bmatrix} F_o \\ 0 \end{Bmatrix} \quad \text{or} \quad \begin{Bmatrix} q'_G \\ q''_G \end{Bmatrix} = \begin{bmatrix} K'_G - \Omega^2 M_G & -K''_G \\ K''_G & K'_G - \Omega^2 M_G \end{bmatrix}^{-1} \begin{Bmatrix} F_o \\ 0 \end{Bmatrix} \tag{29}$$

Once the response (q'_G and q''_G) has been calculated at any frequency Ω, amplitude q_o, corresponding to any degree of freedom, can then be determined as $q_o = \sqrt{(q'_{Gk})^2 + (q''_{Gk})^2}$.

C. Calculation of Modal Damping

The system response is calculated using Eq. (29) over a range of harmonic excitation frequencies. The resonance frequency can be determined and the modal loss factor η, proportional to a ratio of dissipated energy D to the maximum stored energy per cycle $U_{\max}$ can be calculated at this frequency. At resonance, the modal loss factor is a measure of the damping in a mode and is twice the modal damping ratio. It can be shown that the energy dissipated per cycle and the maximum stored energy are given by

$$D_p = \pi\left(q'^T_G K''_G q'_G + q''^T_G K''_G q''_G\right) \quad \text{and} \quad U_{\max} = \tfrac{1}{2}\left(q'^T_G K'_G q'_G + q''^T_G K'_G q''_G\right) \tag{30}$$

so the modal loss factor η can be written as

$$\eta = \frac{1}{2\pi}\frac{D_p}{U_{\max}} = \frac{q'^T_G K''_G q'_G + q''^T_G K''_G q''_G}{q'^T_G K'_G q'_G + q''^T_G K'_G q''} \tag{31}$$

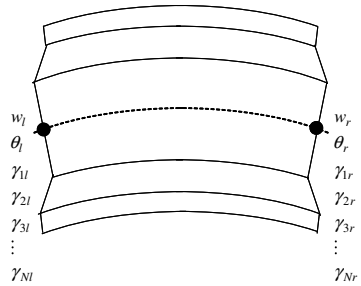

Fig. 2 Schematic of finite element showing the nodal degrees of freedom at the left and right ends.

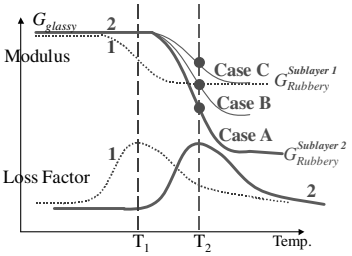

Fig. 3 Variation in shear modulus and loss factor for sublayers 1 and 2 of the damping treatment as a function of temperature.

III. Sample Results and Discussion

Sample simulation results are presented for a 50-cm-long, 20-mm-wide, 4-mm-thick aluminum beam, simply supported at both ends, with constrained-layer damping treatments covering the entire length of both the upper and lower surfaces. The total thickness of the viscoelastic polymer on either surface is 1 mm, and comprises $N = 2$ discrete sublayers of equal thickness (0.5 mm each). The aluminum constraining layer thickness is 1 mm. Figure 3 shows a schematic sketch of the profile of the shear modulus and loss factor variations versus temperature for the two sublayers. Both sublayers have a comparable glassy modulus G_{ref}. At temperature T_1, the sublayer 1 (adjacent to the beam) first enters the transition state, with its modulus dropping below that of sublayer 2 (to a value of $G_{\text{ref}}/5$) and its loss factor increasing appreciably. Sublayer 2 has not yet entered its glass-transition state at temperature T_1 and its modulus remains at G_{ref}. The analysis results (presented in Table 1) show that at temperature T_1, shearing within the polymer is occurring predominantly in the more compliant sublayer 1 (4.46%, compared with 0.89% in sublayer 2). Because this sublayer is also lossy at temperature T_1, a high modal damping (of 7.84%) is observed. At a higher temperature T_2, the sublayer 1 enters the rubbery state, with a further decrease in shear modulus (to $G_{\text{ref}}/20$) and a reduction of the loss factor to negligible values (assumed to be zero).

At temperature T_2, however, sublayer 2 enters the transition state, and so *it* has a significant loss factor. At T_2, if the modulus of sublayer 2 is lower than the rubbery modulus of sublayer 1 (case A in Fig. 3, the modulus of sublayer 2 is assumed to have reduced to $G_{\text{ref}}/50$), most of the shearing occurs in *this* sublayer (8.44%, compared with 3.38% in sublayer 1, as seen in Table 1), and the modal damping remains high (7.01%) because the sublayer undergoing the maximum cyclic shear has dissipative properties. If the modulus of sublayer 2 is $G_{\text{ref}}/20$ at temperature T_2, exactly equal to the rubbery modulus of sublayer 1 (case B in Fig. 3), the cyclic shear strain levels in both sublayers are equal (5.46%, as seen in Table 1). However, because only one of these sublayers is dissipative and the other is nondissipative, the resulting modal damping is somewhat reduced (5.97%). Finally, consider the case when the modulus of sublayer 2 is higher than the sublayer 1 rubbery modulus (case C in Fig. 3, the modulus of sublayer 2 is assumed to have reduced only to $G_{\text{ref}}/10$). Then most of the shear strain is observed in the more compliant sublayer 1 (6.79%, compared with 3.39% in sublayer 2). However, because sublayer 1 undergoing large cyclic shear has a near-zero loss factor and the lossy sublayer 2 experiences relatively lower shear strain levels, the modal damping obtained (4.12% in Table 1) is reduced even further.

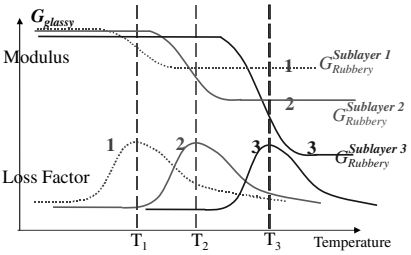

Fig. 4 Desired characteristics of a three-sublayer gradient viscoelastic damping polymer treatment as a function of temperature.

From the preceding results, it is evident that a viscoelastic polymer with properties (and glass-transition temperatures) varying through the thickness can indeed augment structural damping over a broader temperature range than a monolithic treatment. Sublayer 1 alone provides damping augmentation only around T_1, whereas sublayer 2 alone is effective only around T_2. It is also evident that for the maximum possible modal damping at the higher temperature, sublayer 2 (which is entering its transition state at the higher temperature) must have a lower rubbery modulus than sublayer 1 (case A in Fig. 3). Because the glassy moduli of the two sublayers are comparable, this implies that sublayer 2 (which has the higher glass-transition temperature) must have a larger difference between its glassy and rubbery moduli. The glassy modulus of sublayer 2 cannot be significantly reduced, because if it is lower than the modulus of sublayer 1 at temperature T_1, a significant percentage of the shear strain would occur in this nonlossy region (rather than the lossy sublayer 1), and the performance of the treatment at lower temperatures would be compromised.

If an even wider temperature range of effectiveness is desired, a notional sublayer 3 could conceivably have its glass-transition temperature at a higher temperature T_3 ($T_3 > T_2 > T_1$). For maximum effectiveness of the treatment over the temperature range, the rubbery modulus of sublayer 3 would be lower than that of sublayer 2, which would already be lower than that of sublayer 1. The glassy moduli of all the sublayers would be roughly equal. This is depicted in the schematic sketch in Fig. 4.

Next, we consider a case in which the viscoelastic sublayers are commercially available damping polymers. The aluminum base

Table 1 Case study, $N = 2$ sublayers, modal damping, and sublayer shear strains

Temperature	Shear modulus[a]		Loss factor	Shear strain, %	Modal damping, %
T_1		Sublayer 1: $G_{\text{ref}}/5$	0.7443	4.46	7.84
		Sublayer 2: G_{ref}	0	0.89	
T_2	Case A	Sublayer 1: $G_{\text{ref}}/20$	0	3.38	7.01
		Sublayer 2: $G_{\text{ref}}/50$	0.7343	8.44	
	Case B	Sublayer 1: $G_{\text{ref}}/20$	0	5.46	5.97
		Sublayer 2: $G_{\text{ref}}/20$	0.7343	5.46	
	Case C	Sublayer 1: $G_{\text{ref}}/20$	0	6.79	4.12
		Sublayer 2: $G_{\text{ref}}/10$	0.7343	3.39	

[a]Reference (glassy) modulus $G_{\text{ref}} = 12.466$ MPa and Young's modulus of aluminum $E = 71$ GPa

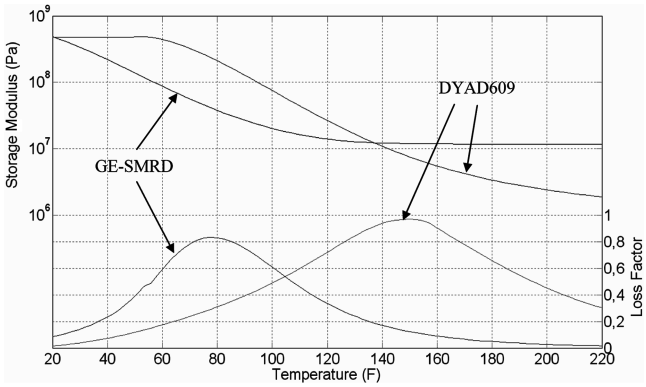

Fig. 5 Variation of the viscoelastic material properties GE-SMRD and DYAD609 as a function of temperature.

beam is 50-cm long, 20-mm wide, and 6-mm thick and simply supported at both ends. The viscoelastic damping layers extending over the length of the upper and lower surfaces of the beam each comprise two sublayers: GE-SMRD (at the surface of the beam) and DYAD-609 (in contact with the constraining layer). The properties of these commercially available viscoelastic materials can be found in [16]. The viscoelastic damping layer is nominally 2-mm thick, with each sublayer being 1 mm in thickness. Each constraining layer is 2-mm thick and is made of composite material: carbon with high modulus (Young's modulus $E = 400$ GPa and $\rho = 1800$ kg $\cdot$ m^{-3}). Figure 5 shows the variation in shear modulus and material loss factor for each of the polymers as a function of temperature. It is seen that GE-SMRD has a peak loss factor at a temperature of 80°F, whereas DYAD-609 reaches its peak loss factor at 130°F. Further, the glassy moduli of both materials are comparable, whereas the rubbery modulus of DYAD-609 (which enters glass transition at a higher temperature) is lower, as desirable for a high-performance, broad-temperature damping treatment. Figure 6 shows damping in the fundamental mode of vibration as a function of temperature. For the treatment comprising the 1-mm GE-SMRD and 1-mm DYAD-609 sublayers, modal damping values of over 15% critical are observed over a temperature range extending from 80–180°F. For 10% critical modal damping, the temperature range of effectiveness goes from 70–210°F. If the viscoelastic damping layer is GE-SMRD alone, the temperature range of effectiveness is much reduced. As seen in Fig. 6, 10% critical modal damping is obtained only over a temperature range of 70–120°F for a 1-mm treatment. If the thickness is 2 mm, the peak damping values are higher, but the temperature range of effectiveness is not significantly increased (compared with the hybrid 2 sublayer treatment). Similarly, if the viscoelastic damping layer is DYAD-609 alone, high damping is obtained at higher temperatures (more than 15% modal damping over a 120–190°F temperature range for the 1-mm treatment and over a 110–190°F range for the 2-mm treatment), but damping levels over the 70–120°F range are low.

Figure 7 shows the variation in strain amplitude in the individual sublayers over the temperature range. It is observed that at

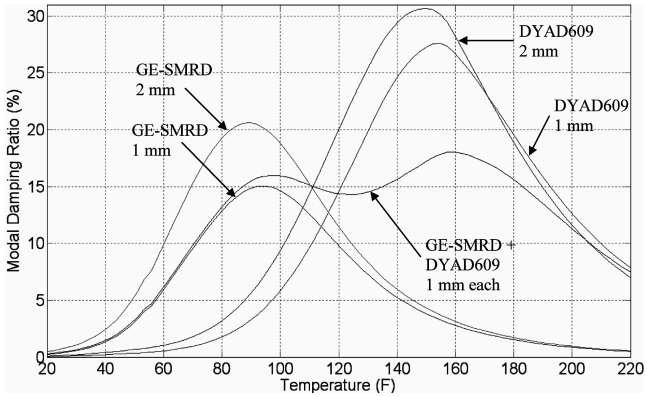

Fig. 6 Modal damping ratio as a function of temperature.

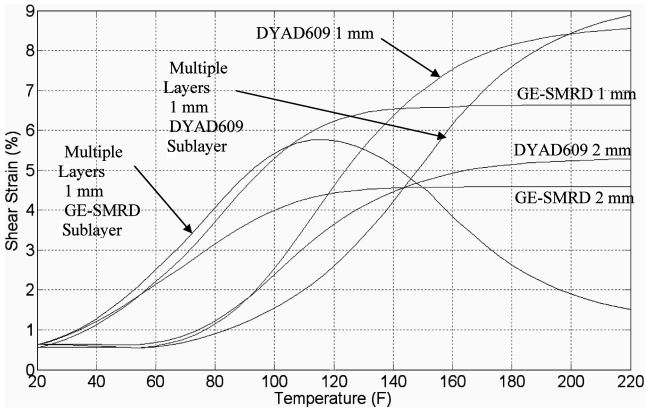

Fig. 7 Variation of the shear strain in viscoelastic layers as a function of temperature.

temperatures lower than 140°F, the shear strain is largest in the GE-SMRD sublayer of the multiple-layer treatment. As the temperature increases beyond 140°F, the shear modulus of the DYAD-609 sublayer has decreased to values lower than that of GE-SMRD (see Fig. 5). Consequently, the shear strain levels in the DYAD-609 sublayer are higher. The effectiveness of damping treatment over the broad temperature range comes from the fact that the shear strain in the GE-SMRD sublayer is larger at lower temperatures, for which it is lossy, and the strain in the DYAD-609 sublayer is larger at higher temperatures, for which its loss factor is high. It is interesting to note that at higher temperatures (greater than 140°F) shear strain in the GE-SMRD sublayer decreases (Fig. 7) even though *its* shear modulus does not (Fig. 5). This is because the shear modulus of the DYAD-609 sublayer becomes *even lower*. In fact, for GE-SMRD alone (1-mm and 2-mm layers) Fig. 7 shows that at temperatures over 140°F, the shear strain levels would be highest because the shear modulus of the material is at its lowest (the rubbery modulus). For DYAD-609 alone (1- and 2-mm layers), the shear strain at low temperatures is very low (Fig. 7) when the material is in the glassy state (Fig. 5). The shear strain starts to increase as the material enters glass transition and then approaches a constant value as the shear modulus approaches the rubbery modulus. Thus, although shear strain variations versus temperature for a monolithic polymer layer may faithfully follow the variation in shear modulus, the strain variation for a multilayer treatment also depends on how the shear moduli of the sublayers compare with each other.

It should be noted that in general, the shear modulus and loss factor of a viscoelastic polymer is also dependent on the shear strain amplitude in the polymer. Thus, the performance of the constrained-layer damping treatment is dependent on the amplitude of excitation ([17]). However, constrained-layer damping studies in the literature have generally neglected the strain-amplitude dependence, which is tantamount to making the assumption that excitation levels are small enough so that the variation in properties with shear strain amplitude are negligible. The same assumption is used in the present study.

IV. Conclusions

This paper presents an analysis for beams with constrained-layer damping treatments having a gradient viscoelastic polymer layer (for which the properties vary through the thickness of the layer). The use of such a gradient viscoelastic polymer can increase the temperature range of effectiveness of the damping treatment. Because the shear modulus of a gradient polymer can vary through the thickness by two–three orders of magnitude, the shear strain cannot be assumed to be uniform. The analysis represents the gradient viscoelastic damping as comprising N discrete sublayers, each with its own properties (that vary with temperature) and each with its own shear degree of freedom.

Simulation results are presented for a pinned–pinned beam with a gradient-polymer constrained-layer damping treatment. The gradient polymer comprises $N = 2$ discrete sublayers. From the

simulation results, it can be concluded that such a treatment can provide damping augmentation over a wider temperature range (than a monolithic viscoelastic layer), and for best performance, the sublayer undergoing glass transition at lower temperature should have a higher rubbery modulus than the sublayer undergoing glass transition at the higher temperature (with the glassy moduli of both sublayers being comparable). This would ensure that over the temperature range of interest, the sublayer that is in the glass-transition state, and therefore having a high material loss factor, is also the one undergoing maximum cyclic shear strain.

References

[1] Baz, A., and Ro, J., "Optimum Design and Control of Active Constrained Layer Damping," *Journal of Vibration and Acoustics*, Vol. 117, No. 2, Apr. 1995, pp. 135–144.

[2] Baz, A., "Optimization of Energy Dissipation Characteristics of Active Constrained Layer Damping," *Smart Materials and Structures*, Vol. 6, No. 3, June 1997, pp. 360–368.

[3] Shen, I. Y., "Hybrid Damping through Intelligent Constrained Layer Treatments," *Journal of Vibration and Acoustics*, Vol. 116, July 1994, pp. 341–349.

[4] Shen, I. Y., "Bending-Vibration Control of Composite and Isotropic Plates Through Intelligent Constrained Layer Treatments," *Smart Materials and Structures*, Vol. 3, No. 1, Mar. 1994, pp. 59–70.

[5] Azvine, B., Tomlinson, G. R., and Wynne, R. J., "Use of Active Constrained-Layer Damping for Controlling Resonant Vibration," *Smart Materials and Structures*, Vol. 4, No. 1, Mar. 1995, pp. 1–6.

[6] Huang, S. C., Inman, D. J., and Austin, E. M., "Some Design Considerations for Active and Passive Constrained Layer Damping Treatments," *Smart Materials and Structures*, Vol. 5, No. 3, June 1996, pp. 301–313.

[7] Lesieutre, G., and Lee, U., "A Finite Element for Beams Having Segmented Active Constrained Layers with Frequency-Dependent Viscoelastics," *Smart Materials and Structures*, Vol. 5, No. 5, Oct. 1996, pp. 615–627.

[8] Gandhi, F., and Munsky, B., "Comparison of Damping Augmentation Mechanisms with Position and Velocity Feedback in Active Constrained Layer Treatments," *Journal of Intelligent Material Systems and Structures*, Vol. 13, No. 5, May 2002, pp. 259–326.

[9] Gandhi, F., and Munsky, B., "Effectiveness of Active Constrained Layer Damping Treatments in Attenuating Resonant Oscillations," *Journal of Vibration and Control*, Vol. 8, No. 6, 2002, pp. 747–775.

[10] Owens, F. S., "Elastomers for Damping over Wide Temperature Ranges," *Shock and Vibration Bulletin*, Vol. 36, No. Pt 4, 1967, pp. 25–35.

[11] Jones, D. I. G., "Design of Constrained Layer Treatments for Broad Temperature Damping," *Shock Vibration Bulletin*, Vol. 44, No. Pt 5, 1974, pp. 1–12.

[12] Nashif, A. D., and Nicholas, T., "Vibration Control by a Multiple-Layered Damping Treatment," *Shock and Vibration Bulletin*, Vol. 41, No. 2, 1970, pp. 121–131.

[13] Jones, D. I. G., Nashif, A. D., and Parin, M. L., "Parametric Study of Multiple-Layered Damping Treatments on Beams," *Journal of Sound and Vibration*, Vol. 29, No. 4, 1973, pp. 423–434.

[14] Remillat, C., and Tomlinson, G. R., "Damping Performance of Constrained Layer Damping Coatings Based on Gradient Polymer Materials," *ISMA25: International Conference on Noise & Vibration Engineering* [CD-ROM], Dept. of Mechanical Engineering, Katholieke Univ. Leuven, Leuven, Belgium, Sept. 2000.

[15] Remillat, C., and Tomlinson, G. R., "A Study on Gradient Polymer Coatings Used as Damping Coatings: Focus on Free Layer Damping," *Proceedings of the ASME, Noise Control and Acoustics Division—2000*, Vol. 27, American Society of Mechanical Engineers, New York, 2000, pp. 517–524.

[16] Nashif, A. D., Jones, D. I. G., and Henderson, J. P., *Vibration Damping*, Wiley, New York, 1985.

[17] Gandhi, F., "Influence of Nonlinear Viscoelastic Material Characterization on Performance of Constrained Layer Damping Treatment," *AIAA Journal*, Vol. 39, No. 5, May 2001, pp. 924–931.

C. Pierre
Associate Editor